Chaos, Solitons and Fractals 168 (2023) 113140

Contents lists available at ScienceDirect

Chaos, Solitons and Fractals

journal homepage: www.elsevier.com/locate/chaos

Double stochastic resonance in neuronal dynamics due to astrocytes

Tugba Palabas [a], Joaquín J. Torres [b], Matjaž Perc [c,d,e,f,g], Muhammet Uzuntarla [h,*]

[a] Department of Biomedical Engineering, Zonguldak Bulent Ecevit University, 67100, Zonguldak, Turkey
[b] Department of Electromagnetism and Physics of the Matter and Institute Carlos I for Theoretical and Computational Physics, University of Granada, Granada, E-18071, Spain
[c] Faculty of Natural Sciences and Mathematics, University of Maribor, Koroška cesta 160, 2000 Maribor, Slovenia
[d] Complexity Science Hub Vienna, Josefstädterstraße 39, 1080 Vienna, Austria
[e] Department of Medical Research, China Medical University Hospital, China Medical University, 404332 Taichung, Taiwan
[f] Alma Mater Europaea, Slovenska ulica 17, 2000 Maribor, Slovenia
[g] Department of Physics, Kyung Hee University, 26 Kyungheedae-ro, Dongdaemun-gu, Seoul, Republic of Korea
[h] Department of Bioengineering, Gebze Technical University, 41400, Kocaeli, Turkey

ARTICLE INFO

Keywords:
Stochastic resonance
Astrocyte
Dressed neuron

ABSTRACT

A continuously growing body of evidence indicates that astrocytes, which is the most abundant sub-type of glial cells in the nervous system, not only provide structural and metabolic support to neurons, but also they are essential sentinels and dynamic modulators of neuronal and synaptic functions. However, the potential constructive role of astrocytes in information processing at the neuronal and synaptic level, and especially also in the presence of different noise sources in the neural system, is yet unclear. With this in mind, we here study the phenomenon of stochastic resonance – the enhanced detection of weak signals in the presence of noise – in neuronal dynamics by means of a mathematical model that includes interactions between the neuron and the astrocyte. We show that astrocytes may evoke a second peak in the neuronal detection of weak signals in dependence on the noise intensity, which is the hallmark of double stochastic resonance. We explore in detail the mechanisms underlying this discovery, in particular focusing on the determinants of astrocytic function and their role in the emergence of the second stochastic resonance peak. Our research thus provides fundamental insights into the possible roles of astrocytes in inherently noisy neuronal information processing.

1. Introduction

A typical characteristic property of all biological systems, their parts or populations is the existence of non-linear processes affecting their intrinsic dynamics and functioning, in such a way that these systems can generate different outputs which can propagate in space and time, some of them unpredictable, for small variations on the system's influences. Even though non-linearity is commonly expressed as an undesirable feature which allow, e.g., for the propagation of effects without damping, it has been demonstrated that it plays an essential role for the ability and adaptation observed in biological systems [1,2].

A prominent example of such living systems using advantage of non-linearity is the nervous system of animals. The brain of mammals, for instance, has a complex network structure which is the result of different biophysical non-linear processes occurring during its development [3–5], that allow it to optimally perform many sophisticated tasks (e.g. information processing, memory acquisition and consolidation, attention and perception to name a few) despite the complicated and varied interactions among neurons and of these with the noisy environment. For instance, animals continuously are receiving behaviorally essential data from their surrounding through sensory neurons (e.g. visual, olfactive or auditory), which provide some information about navigation, communication and preying in order to survive. In most of situations, such relevant information is continuously perturbed by other signals, sometimes uncorrelated, originated in a constantly varying environment. Capturing relevant data from such varying noisy background of stimuli sometimes requires properly decoding sub-threshold weak signals which may be an indicator of a possible emerging issue, such as environmental hazards or predator and prey localizations. A complete understanding of the mechanisms by which weak signals can be processed in a background of noisy activity is crucial to decipher how sensory relevant information is processed by human brain. With this aim, recently, there was an increasing interest in neuroscience research to study the underlying mechanisms that help to enhance such weak signals from its noisy surrounding activity [6–10]. In particular, experimental and theoretical studies have revealed

* Corresponding author.
E-mail address: muzuntarla@gtu.edu.tr (M. Uzuntarla).

https://doi.org/10.1016/j.chaos.2023.113140
Received 17 December 2022; Accepted 10 January 2023

that central nervous system neurons, like sensory neurons, can capture and amplify sub-threshold signals through several non-linear resonance mechanisms that have previously been discovered in some other natural and physical systems [11–16].

In the context of resonance-based weak signal capturing and enhancement in non-linear systems, a notable phenomenon is the so called stochastic resonance (SR) whereby the response of the neuronal system under the action of a subthreshold input signal can be amplified by the presence of an optimal level of noise [17–22]. Up to date, many studies have been conducted to examine the effect of SR phenomenon on neural dynamics at both single neuron and population level under various biophysical conditions [23–31]. Indeed, the findings suggest that weak signal amplification is possible in the presence of the moderate level of noise in neural environment. In addition, it has been widely reported that the efficiency of SR can also be tuned by many biophysical properties of neural systems such as network structure, dynamics of ion concentrations and heterogeneity [32–36]. Moreover, some studies have also indicated that biophysical processes at the synapses involved in neurotransmitter trafficking, release and recycling, and which are in the base of short-term synaptic plasticity, strongly influence the SR characteristic of neural circuits inducing, for instance the appearance of bi-modal SR resonances while processing weak signals [17,24,37–39].

In most previous modeling studies on SR in neural systems, including specific brain areas and neuronal populations, neurons have been recognized as the most prominent cell types for information processing in the brain, and most of the times uncorrelated neural activity from other areas has been considered as the sole source of noise to induce neuronal stochastic behavior. However, such an assumption in neuronal systems modeling lacks in imitating real biophysical conditions and it does not provide a clear understanding of SR behavior in terms of concrete biological mechanisms. Thus, recently other possible sources of noise that can induce intriguing SR phenomena have been considered including ionic channel noise and synaptic noise [40,41], but still we are far from understanding all biological aspects that can induce SR in actual neural systems. Hence, for instance, findings from experimental studies both *in vivo* and *in vitro* have revealed that glia cells are also important elements in neuronal systems, which are initially thought to serve only metabolic and structural support for neurons and synapses [42–47]. Namely, a glial cell mass with embedded neurons provides a more realistic picture of the brain tissue.

Astrocytes are the most prevalent glial cells in the brain. Experiments have shown that these star-shaped cells actively participate in a large variety of central nervous system functions including synaptogenesis, neuronal communications and synaptic plasticity [48,49]. In particular, during synaptic transmission *dressed* neurons [50–53], namely neurons surrounded by astrocytes, release neurotransmitters such as glutamate that are partially bound by glutamate receptors at the astrocytes membrane. This binding process induces calcium release from internal stores increasing its concentration in the astrocyte cytosol and causing the subsequent release of astrocyte gliotransmitter (e.g. D-serine, astrocytic glutamate, ATP) into synaptic cleft, affecting both the presynaptic and the postsynaptic neurons and consequently modulating the synaptic transmission [54–56]. This indicates that astrocytes are able to contact bidirectional communication with dressed neurons, based on mutual glutamatergic signaling pathways.

An interesting question to address in the present context is if such complex interaction between pre and postsynaptic neurons and astrocytes, which constitutes the so called tripartite synapse, can affect optimal detection of weak signals in a background of noise through the SR mechanism. This issue has been systematically studied in recent years using theoretical models. For instance, Liu and Li have modeled four different neuronal network motifs in a two-dimensional astrocyte field with mutual neuron–astrocyte interactions and discussed the impacts of astrocytes on SR in these building blocks of neuronal networks [57]. In an another recent study, by modeling a system containing a neuron and an astrocyte, Erkan et al. investigated how weak signal transmission performance of the neuron changes in the presence and absence of the astrocyte [58]. They have found that the neuron's performance for detecting weak signals at an optimal noise level of the environment is significantly improved in the presence of astrocytes.

These intriguing findings have motivated us to further investigate in the present work the phenomenon of SR in a bipartite neuron–astrocyte system using a FitzHugh–Nagumo model for neuronal dynamics under more realistic conditions. For example, the above-mentioned existing studies investigating the effect of astrocyte on SR have not evaluated the inhibitory effect of astrocytic feedback on the presynaptic neuron. Moreover, these studies have not analyzed in detailed the relevant parameters although the strength of this feedback is highly dependent on the internal dynamics of astrocyte. Thus, here, we explore the weak signal detection performance of the dressed neuron under the variation of different biologically-plausible intrinsic astrocytic factors as the production and degradation rate of inositol trisphosphate, and neuron–astrocyte coupling strength. Our results reveal that the interaction between neuron and astrocyte may induce the emergence of double SR phenomenon similar to those already found in neural dynamics due to different biophysical factors [28,59]. We show that this intriguing effect can be modulated by internal dynamics of the astrocyte and clarify the underlying mechanism that give rise to double SR in terms of the non-monotonic variation of astrocytic feedback with noise.

2. Model and methods

A schematic illustration of the system under study in the present work is depicted in Fig. 1. This consists of a neuron–astrocyte pair, which is driven by a weak periodic signal and subjected to a noisy background activity originated from the network or other biophysical factors. As seen in the plot, the neurotransmitter release into the synaptic cleft is sensed by mGluR receptors of the astrocyte, which then induces movement of gliotransmitter molecules towards the synaptic space due to the increase of $IP3$-mediated Ca^{2+} concentration in the intracellular space.

To investigate the stochastic resonance phenomenon in the response of the neuron, we use the Fitzhugh–Nagumo (FHN) equations to simply model the neural dynamics, defined as follows [60–62]:

$$\epsilon \frac{dV_m}{dt} = V_m - \frac{1}{3}V_m^3 - \omega + \sqrt{2D}\xi(t) + I_{ext} \tag{1}$$

and

$$\frac{d\omega}{dt} = V_m + a_e + \lambda I_{astro} \tag{2}$$

where V_m is the fast variable that accounts for the electrical activity of the neuron and ω is the slow recovery variable which can be biophysically related with the activity of several types of membrane channel proteins, e.g. potassium channel kinetics [63]. ϵ characterizes the time-scale separation between fast (V_m) and slow (ω) variables of the neuron model and it is fixed to 0.01 in this study. The excitability level of the neuron is determined with the bifurcation parameter a_e where the FHN neuron is excitable for $|\ a_e\ | \geq 1$, while for $|\ a_e\ | < 1$, the system exhibits an oscillatory (limit cycle) behavior generating a periodic spike sequence. In our analysis, the bifurcation parameter is set slightly outside the oscillatory regime to $a_e = 1.03$. $\xi(t)$ represents the Gaussian white noise with zero mean and intensity D which accounts, for instance, for uncorrelated input activity from the surrounding arriving to the neuron and affecting its excitability. The sub-threshold input signal, which could be related with environmental weak stimuli reaching to the sensory neurons in actual brains, is defined by $I_{ext} = Asin(\omega_s t)$ with amplitude A and angular frequency ω_s.

The I_{astro} term in Eq. (2) is an inhibitory feedback to the presynaptic neuron, which may be originated from the release of astrocytic gliotransmitters, e.g. ATP/Adenosine, that can bind to A1R channels and cause the opening of the potassium channels on the presynaptic neuron.

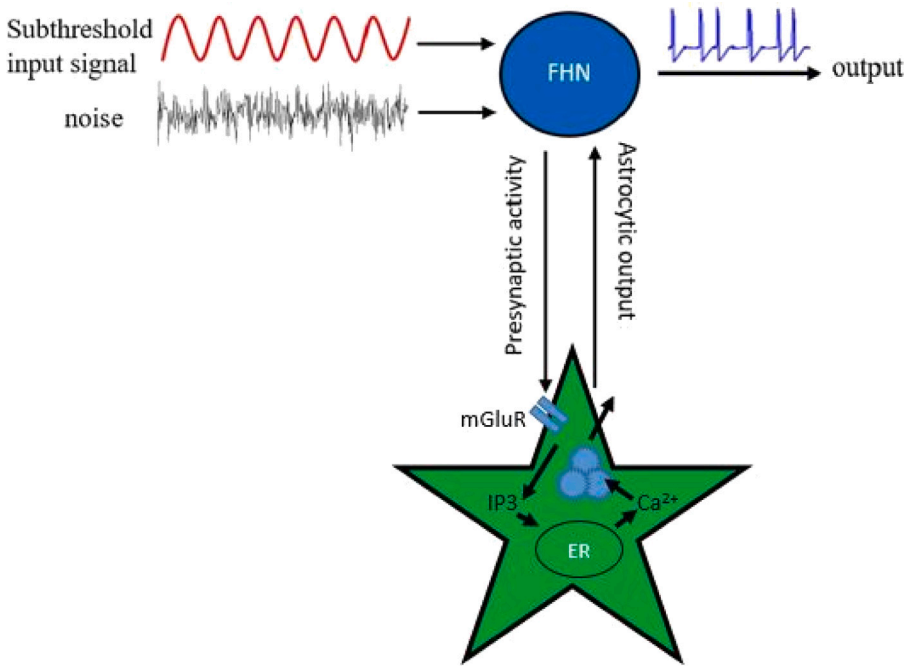

Fig. 1. The schematic illustration of the neuron–astrocyte coupled system used in the present study. This bipartite system is composed of a presynaptic neuron and an astrocyte that enwrapes the synapse. The neuron (in blue) receives a sub-threshold input signal, and it is also exposed to the noise which may be originated from the synaptic background activity or other biophysical factors (in black). The release of neurotransmitter from the neuron acts both on the synaptic terminal as well as on astrocytic receptors mediating intracellular $IP3$ and calcium elevation in astrocyte. This triggers the release of gliotransmitters that bind with the presynaptic terminal receptors resulting in the emergence of an astrocytic feedback I_{astro} that modulates the excitability of the neuron. (For interpretation of the references to color in this figure legend, the reader is referred to the web version of this article.)

This fact influences the intracellular potassium dynamics of the neuron which affects both the generation of spikes near the synapse (through hyperpolarization) and the subsequent synaptic transmission [64,65]. Since the I_{astro} is a slow current, we coupled it with the slow variable ω of the model neuron equations (since ω can also account for potassium concentration dynamics in the presynaptic neuron) and its influence is adjusted with the coupling strength λ. I_{astro} is indirectly originated by the dynamical changes in the intrinsic calcium (Ca^{2+}) concentration of the astrocyte that causes gliotransmitter release at the synaptic cleft. This happens after astrocyte cytosolic Ca^{2+} level increase from the intrinsic stores which occurs depending on inositol 1,4,5-triphosphate ($IP3$) production. The later is triggered by the binding of glutamate (Glu) released into the synaptic cleft to the metabotropic glutamate receptors (mGluRs) of the astrocyte, when the neuron fires an action potential. To model this briefly introduced processes, we assume that the production of $IP3$ in the astrocyte obeys the following dynamics [66]:

$$\frac{d[IP3]}{dt} = \frac{1}{\tau_{IP3}}([IP3]^* - [IP3]) + r_{IP3}\frac{1}{1+e^{(\theta_s - V_m)/\sigma_s}} \tag{3}$$

where the first term on the right-hand side of the equation represents the degradation in intracellular $IP3$ concentration whereas the second one, defined by a sigmoid function with steepness σ_s, refers to its production which is triggered when V_m exceeds the threshold voltage θ_s. Based on experimental studies [67–69], the $IP3$ equilibrium concentration $IP3^*$ and the rate of $IP3$ degradation $1/\tau_{IP3}$ are set as 160 nM and 0.00014 ms^{-1}, respectively. The parameter r_{IP3} denotes the astrocyte $IP3$ production rate in response to each spike activity of the presynaptic neuron [70].

The cytosolic Ca^{2+} concentration of the astrocyte is modeled by using the Li–Rinzel (LR) equations [71] which describe the Ca^{2+} dynamics with three different fluxes: $J_{channel}$ is Ca^{2+} flux from Endoplasmic Reticulum (ER) lumen to the intracellular space via $IP3R$ channels, J_{pump} is the Ca^{2+} flux from cytosol into ER through ATP-dependent pumps and J_{leak} is the leakage flux from the ER to the cytosol due to difference in Ca^{2+} concentrations between the intracellular stores and the cytosol. Then, the Ca^{2+} dynamics part of the model consists of the following differential equations [71,72]:

$$\frac{d[Ca^{2+}]}{dt} = -J_{channel} - J_{pump} - J_{leak} \tag{4}$$

and

$$\frac{dq}{dt} = \alpha_q(1-q) - \beta_q q. \tag{5}$$

Here, q refers to the fraction of activated $IP3$ receptor channels (IP3Rs) calculated according to activation α_q and inactivation β_q rates of IP3Rs (see also [66]). The definitions of calcium flows $J_{channel}$, J_{pump} and J_{leak} across the ER are as follows:

$$J_{channel} = c_1 v_1 m_\infty^3 n_\infty^3 q^3([Ca^{2+}] - [Ca^{2+}]_{ER}) \tag{6}$$

$$J_{pump} = \frac{v_3([Ca^{2+}]^2)}{k_3^2([Ca^{2+}]^2)} \tag{7}$$

$$J_{leak} = c_1 v_2([Ca^{2+}] - [Ca^{2+}]_{ER}) \tag{8}$$

where

$$m_\infty = \frac{[IP3]}{[IP3]+d_1}, \qquad n_\infty = \frac{[Ca^{2+}]}{[Ca^{2+}]+d_5} \tag{9}$$

and

$$[Ca^{2+}]_{ER} = \frac{c_0 - [Ca^{2+}]}{c_1}. \tag{10}$$

Lastly, the astrocytic inhibitory feedback is defined as a function of intracellular Ca^{2+} concentration as follows [66]:

$$I_{astro} = 2.11 ln(y)\Theta(ln(y)), \qquad y = [Ca^{2+}] - 196,69 \tag{11}$$

where y is the amount of Ca^{2+} above the threshold level and Θ represent a Heaviside step function: $H(x) = 1$ for $x > 0$, and $H(x) = 0$ for $x < 0$. The values of other astrocyte parameters appearing in above model equations are listed in Table 1 [73].

Table 1
Astrocyte standard parameters.

Parameter	Value	Description
c_1	0.185	Ratio of ER volume to cytosol volume
v_1	6 s^{-1}	Maximum Ca^{2+} channel flux
v_2	0.11 s^{-1}	Ca^{2+} leak flux constant
v_3	0.9 μM s^{-1}	Maximum Ca^{2+} uptake
k_3	0.1 μM	SERCA activation constant
d_1	0.13 μM	$IP3$ dissociation constant
d_5	0.08234 μM	Ca^{2+} activation dissociation constant
c_0	2.0 μM	Cytosolic free Ca^{2+} concentration

The response of the neuron to the weak signal is quantified by means of the Q factor which is a measure of the Fourier spectrum of V_m at the frequency ω_s [74,75]:

$$Q = \sqrt{Q_{sin}^2 + Q_{cos}^2} \tag{12}$$

where Q_{sin} and Q_{cos} are computed via the Fourier coefficients:

$$Q_{sin} = \frac{\omega_s}{2n\pi} \int_0^{2n\pi/\omega_s} 2V_m(t) sin(\omega_s t) dt \tag{13}$$

and

$$Q_{cos} = \frac{\omega_s}{2n\pi} \int_0^{2n\pi/\omega_s} 2V_m(t) cos(\omega_s t) dt \tag{14}$$

and where n is the number of stimulus periods covered during the integration time. The described mathematical model is integrated numerically using the forward Euler method with a time step $\delta t = 0.005$. For statistical accuracy, all computational results are presented below have been averaged over 50 realizations of the coupled system for any given set of the model parameters.

3. Results

In what follows, we systematically analyze the impact of the astrocyte dynamics on the weak signal detection performance of the dressed-neuron in the considered bipartite system (Fig. 1). To demonstrate the role of astrocyte explicitly, we first consider the case of an isolated neuron where its connection with astrocyte is blocked and assumed that it is only subjected to weak periodic signal and noise. Obtained results are presented in Fig. 2 which depicts, in panel (a), the variation of Fourier coefficient Q versus noise intensity D. It is seen that Q follows a bell-shaped performance curve, so-called SR, reaching maximum values for a particular range of D. This indicates that the presence of an optimal noise level in the system may result in strong correlation between the output spike pattern and the weak input signal. To explore such correlation and the underlying mechanism of the SR in the considered model neuron, we plot output voltage traces of the isolated neuron along with the weak input signal in panel (b) for five different selected points on the SR curve as marked with b_1–b_5 in panel (a). It is seen in the left side of panel (b) that the spiking activity of the model neuron exhibits a pronounced increase as the noise intensity increases. Since such a long-term spiking behavior of the neuron seems to be noisy and it is hard to follow whether the neuron fires spikes in a manner correlated with the weak signal, we explore randomly selected epochs (blue boxes) of the firing patterns and plot them on the right panels of Fig. 2(b). It is obvious that the isolated neuron is almost in a quiescent state for small values of D because such noise levels (b_1) are not enough strong to frequently excite the neuron. With the increase of noise (at b_2), the neuron still fires sparsely but we observe that all the firings occur almost at the same phase of the weak periodic input signal, indicating that such noise levels trigger a phase-locked neuronal firing mode [76,77], which results in an increase of the correlation coefficient Q (see panel (a)). It should be noted that this phase-locked activity form was observed not only during the observed time interval, but also throughout the entire activity period. With further increase of noise (at b_3), the phase-locked mode still exists in neural dynamics but with rare false spikes occurring at different phases of the stimulus (labeled with red asterisks). It can be said that the increased spiking rate along with the phase-locked firing mode for such an optimal noise level result in a strong correlation between neuronal output and the input signal. When the noise strength increases beyond the optimal level, we observe that the phase-locking mode disappears from neural dynamics and the number of false spikes increases significantly (at b_4 and b_5). This causes a dramatical decrease in correlation between input and output of the considered system as can be understood from variation of Q at such noise levels in panel (a).

After introducing and explaining the SR effect in our isolated model neuron dynamics above, we now turn our attention to the role of astrocyte on weak signal detection performance of the dressed neuron. Following the same protocol as in the case of isolated neuron, we computed the variation of Q as a function of D for a fixed coupling strength (λ) among astrocyte and neuron dynamics. Fig. 3(a) features the obtained results. Interestingly, it is seen that a double SR with two distinct peaks centered at different noise ranges occurs in the response of the dressed neuron. To express the underlying mechanism of this double SR, we plot astrocytic feedback current (in cyan) and output voltage traces of the dressed neuron (in black) along with weak input signal (in green) in panel (b) for six different selected points on SR curve (marked with b_1–b_6).

Compared with the isolated neuron, it is seen in the left column of panel (b) that there exists a dramatic variation in the firing profile of the dressed neuron as the noise strength D increases. More precisely, the dressed neuron exhibits sparse, burst-like and intense firing behaviors at low, moderate and high levels of noise, respectively. We believe that such astrocytic feedback induced multi-firing modes in neuron dynamics may determine the emergence of double SR phenomenon. For instance, when the noise level is low, the firing rate of the neuron is not enough for the efficient release of Glu molecules in the synaptic cleft, which then cannot be uptake by the astrocyte, so the production of IP3 molecules within the astrocyte decreases. Accordingly, the IP3-dependent calcium concentration in the astrocyte does not reach the required level to generate astrocytic output in the form of released gliotransmitters [78]. In practice, this results in lack of astrocytic feedback and therefore at low noise levels, the neuron fires sparsely and uncorrelatedly as in the case of an isolated cell (see panel b_1) resulting in low Q.

On the other hand, when the neural activity increases further due to increased noise an oscillating astrocytic output emerges (see left panels of b_2–b_4) arising from the excitatory–inhibitory coupling between neuron and astrocyte dynamics. In our model, it should be noted that while neuronal activity excites the astrocyte to generate an output signal, the astrocytic output lowers the excitability level of the neuron. This push–pull mechanism results in a burst-like neuronal firing regime (b_2–b_3), which includes noise-induced firing periods and astrocytic output signal induced silent periods, or spiking regime (b_4) with only a few local silences in firing activity. As can be seen in the right panels of b_2–b_4 the dressed neuron acts as in the case of isolated cell within the firing periods of these patterns, exhibiting phase-locked spiking activity at optimal noise strength (b_3). This indicates that the emergence of the first resonance peak of double SR is based on the same mechanism as in the case of isolated neuron. Besides, the silent periods in the burst-like regime result in a decrease in resonance peaks compared with the isolated case, which refers to a lower weak signal detection quality (cf. Y-axis in panels Fig. 2(a) and Fig. 3(a)).

Finally, the second resonance peak occurring at large noise region (b_4–b_6) can be understood by considering again the competition between neuronal excitation and astrocytic inhibition. Namely, the increased noise first results in very high neural activity that induces a quick inhibitory astrocytic feedback signal to the neuron. Since the noise is very large, the inhibition from astrocyte cannot silence the large noise-induced firing of the neuron but it decreases the spiking

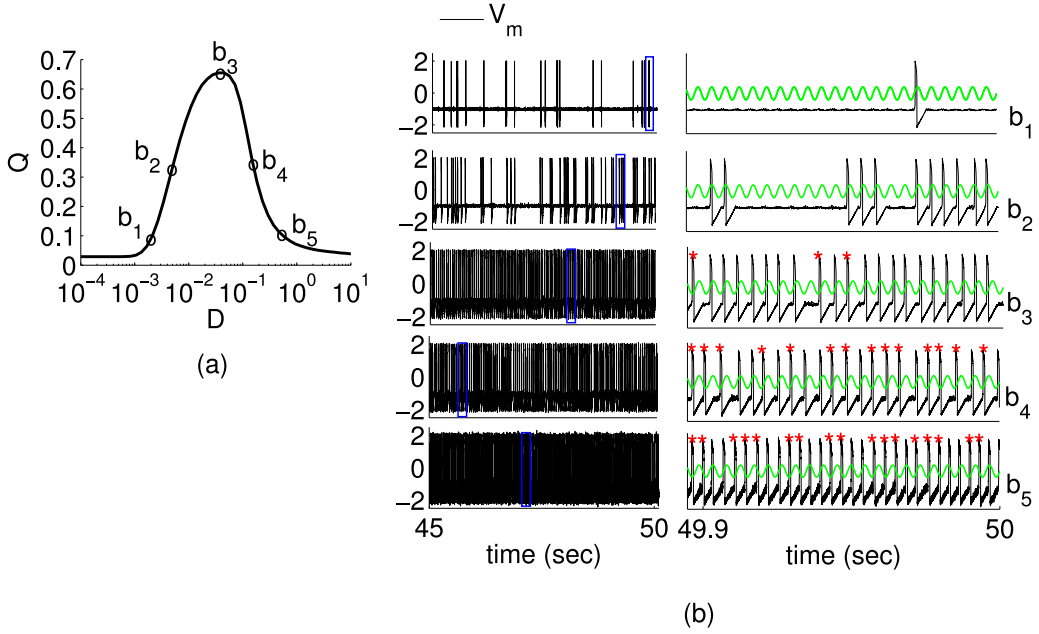

Fig. 2. Weak signal detection performance of the isolated neuron where its connection with astrocyte is blocked and assumed that it is only subjected to weak periodic signal and noise. (a) Variation of Fourier coefficient Q with noise intensity D. (b) The voltage traces (black) of the neuron at various noise intensities marked with b_1–b_5 in panel (a). Here, while the first column shows long term activity of the model neuron, the second column demonstrates randomly selected short epochs (blue boxes) of the same voltage traces shown in the left column along with the weak periodic input signal (green). As can be inferred from panels, a stable phase-locked firing mode exists in neural dynamics until the noise reaches a certain level (b_3). With further increase of noise beyond this level, the false spikes occurring at negative phase of the stimulus (labeled with red asterisk) decrease the correlation between the input signal and neuronal output. The frequency ω_s and amplitude A of subthreshold signal are adjusted as 1.42 and 0.01, respectively. (For interpretation of the references to color in this figure legend, the reader is referred to the web version of this article.)

activity slightly by lowering the neuronal excitability further away from the firing threshold. The overall effect is that the neuron still continues triggering the astrocyte to generate an output which reaches its maximum saturating level for very large noise levels. Such saturating level is unable to cease the spiking activity as for low level of noise described above and results in an almost constant maximum inhibitory astrocytic signal as noise increases further (see blue cyan lines in left panels marked with b_5–b_6 of Fig. 3(b)). With such a stable inhibitory feedback, the neuron achieves a stable excitability state where it becomes less excitable than the isolated neuron. Then, as shown in right panels of b_4–b_6, an optimal large noise induces the same phase-locked spiking mode in neuron dynamics, resulting in the emergence of second resonance peak of the double SR curve.

The above results clearly demonstrate that dynamics of an astrocyte may induce double SR as well as may provide a control mechanism for such resonance behavior. In order to further elaborate on this assessment, we first investigate the effect of coupling strength between the neuron and astrocyte by tuning the λ in Fig. 3. Obtained results are presented in Fig. 4(a). It is evident that the dressed neuron can exhibit double SR phenomenon only for an optimal range of λ and its effect is more pronounced on the second resonance peak. More precisely, with the decrease of λ, the second resonance peak first shifts to the left (less noise) and then collapses with the first resonance peak resulting in disappearance of double SR. On the other hand, although the increase of λ does not effect significantly the width and location of the first resonance peak, the second resonance peak shifts to the right (high noise) with decreasing maximums and finally completely disappears when λ exceeds a certain value (see red line in the left column).

To understand how λ has such a modulatory role on the resonance behavior, we plot the I_{astro} feedback signal in panel (b) for various representative values of λ at critical noise regions where the SR curves reach their peaks (marked with D_1 and D_2 noise regions in panel (a)). In D_1 noise region, it is seen that I_{astro} exhibits an oscillatory profile which, as explained above, induces burst-like firing behavior in neuron dynamics if the astrocytic inhibition is strong enough to silence the neuron for a certain period. Considering this, one can interpret that the insignificance of λ on the first resonance peaks in D_1 noise region arises from the fact that the astrocytic inhibition is very strong and such noise levels cannot overcome this inhibition. Thus, the neuron exhibits almost exactly the same burst-like firing patterns for all considered values of λ resulting in similar signal detection performance in D_1 noise region. On the other hand, in D_2 noise region, variation of λ causes various I_{astro} profiles which are first a DC-like with increasing amplitude as λ increases and then an oscillatory mode for very high level of λ. (see bottom panel in Fig. 4b). Recall that this profile change occurs due to the fact that λ induced amplified inhibition disrupts balanced state in the excitatory–inhibitory interaction between neuron and astrocyte. Since the required stable neuronal excitability condition for the emergence of second resonance peak does not exist anymore with the emergence of oscillatory I_{astro}, double SR phenomenon disappears from system behavior at large values λ. The decrease and shift in second resonance peaks with the increase of λ can be understood by considering the optimal noise requirements to trigger the phase-locked spiking behavior. Since the increased inhibition with large λ requires more noise, the second resonance occurs at higher noise levels which cause the occurrence of false spikes more frequently in phase-locking behavior. These increased number of false spikes decreases the maximums in resonance peaks.

Next, we extend our analyses by investigating the influence of internal dynamics of the astrocyte on the double SR phenomenon. To do so, we explore the weak signal response of the dressed neuron under the variation of r_{IP3} by scanning the lower and higher values of $IP3$ production rates. Obtained results are presented in Fig. 5(a). It is seen that the double SR behavior appears only for moderate values of r_{IP3} and it turns into classical single peak SR at low and high $IP3$ production rates: in fact, the first and second resonance peaks in double SR are suppressed respectively with increased and decreased values of r_{IP3}. To improve our understanding on the effect of r_{IP3} on resonance curves, we plot the traces of the I_{astro} feedback signal in panel (b) for various representative values of r_{IP3} in D_1 and D_2 noise

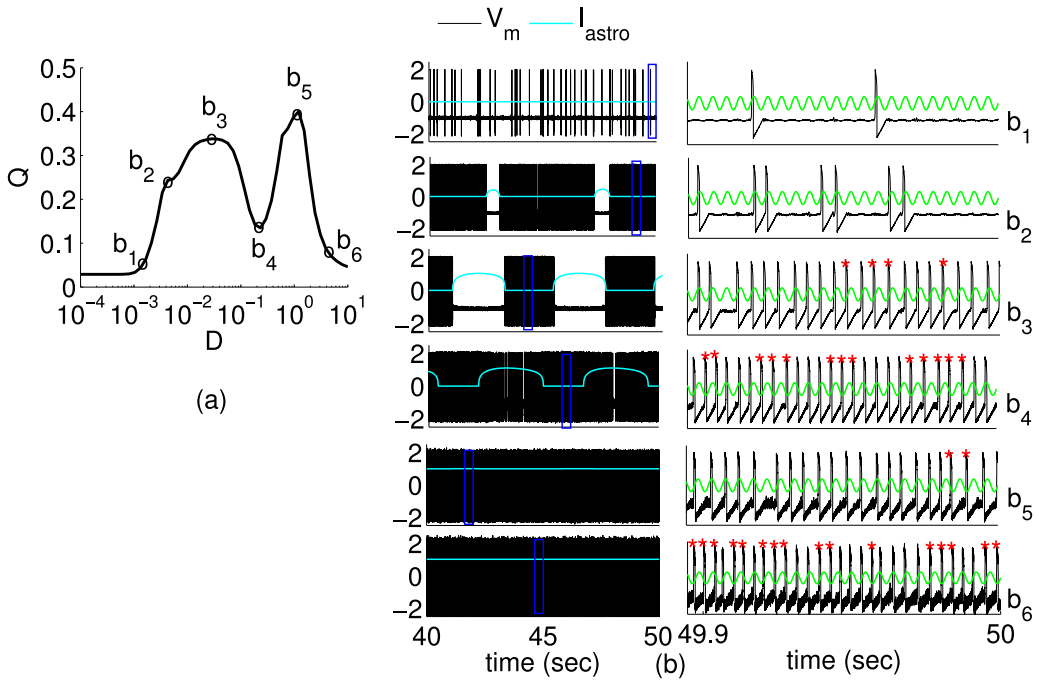

Fig. 3. Emergence of double stochastic resonance in a dressed neuron. (a) Fourier coefficient versus D for a fixed coupling strength $\lambda = 0.009$ and $IP3$ production rate $r_{IP3} = 1.25$. (b) Following the same description as in Fig. 2, we plot long (left column) and short term (right column) voltage traces (black) of the neuron at various noise intensities marked with b_1–b_6 in panel (a). The astrocytic output signal (cyan) having slow dynamics and the relatively faster weak periodic input (green) are also superimposed into the plots. As explained in the main text, the underlying mechanism for the emergence of double SR in the dressed neuron is based on the astrocytic modulation of the neuronal excitability that triggers the phase-locked spiking mode in neuron dynamics at two different noise intensities. (For interpretation of the references to color in this figure legend, the reader is referred to the web version of this article.)

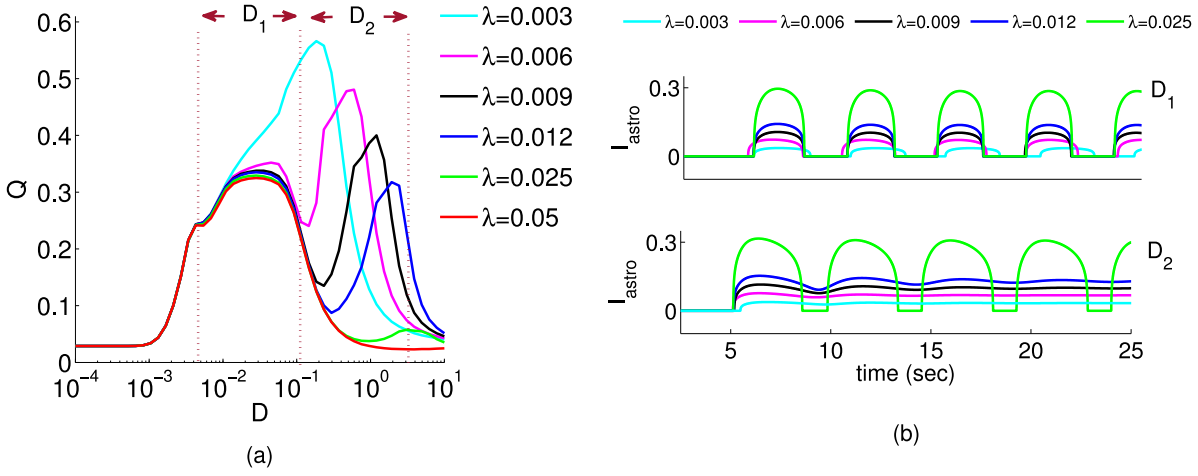

Fig. 4. The influence of neuron–astrocyte coupling strength on the weak signal detection performance. (a) Q versus D for different values of λ and a fixed $r_{IP3} = 1.25$. (b) Temporal profiles of I_{astro} emerging in low (D_1) and high (D_2) levels of D defined in panel (a). Astrocytic feedback is shown for five selected λ values that are the same color coded with the SR curves in the left panel. Note that the corresponding astrocyte activity with very high amplitude and oscillating profile is not shown in the right panel, as the second resonance peak disappears when the lambda is too large, as seen in the left panel. (For interpretation of the references to color in this figure legend, the reader is referred to the web version of this article.)

regions where the SR curves reach their peaks (see panel (a)). It is seen that I_{astro} emerges in D_1 noise region with an oscillating profile and the increase in r_{IP3} enlarges both lifetime and amplitude of I_{astro}. Such modulation of astrocytic feedback indicates that the oscillatory I_{astro} induced burst-like neuronal firing activity patterns includes longer silent periods resulting in decreased weak signal detection performance as r_{IP3} increases in D_1 noise region. On the other hand, in D_2 high noise region, I_{astro} exhibits first an oscillatory profile and switches to DC-like profile when r_{IP3} increases, as it is seen in bottom panel of Fig. 5(b). Also note that I_{astro} does not change very much with further increase in r_{IP3}, saturating almost at a constant level. These observed profile switch and saturation behaviors in I_{astro} clearly explain why the second resonance peaks tends to disappear as r_{IP3} decreases.

Then, to gain a better understanding about the effect of astrocyte on weak signal detection performance, in Fig. 6, we illustrate the joint role of the degradation rate of $IP3$, i.e. $1/\tau_{IP3}$, and noise level (D) in a 3D plot of the Q behavior. When τ_{IP3} is very large (i.e. degradation of IP3 is slow), the diffusion process of $IP3$ which is responsible for Ca^{2+} release from intracellular stores occurs very slowly. As a consequence, these extremely slow kinetics are not enough to induce

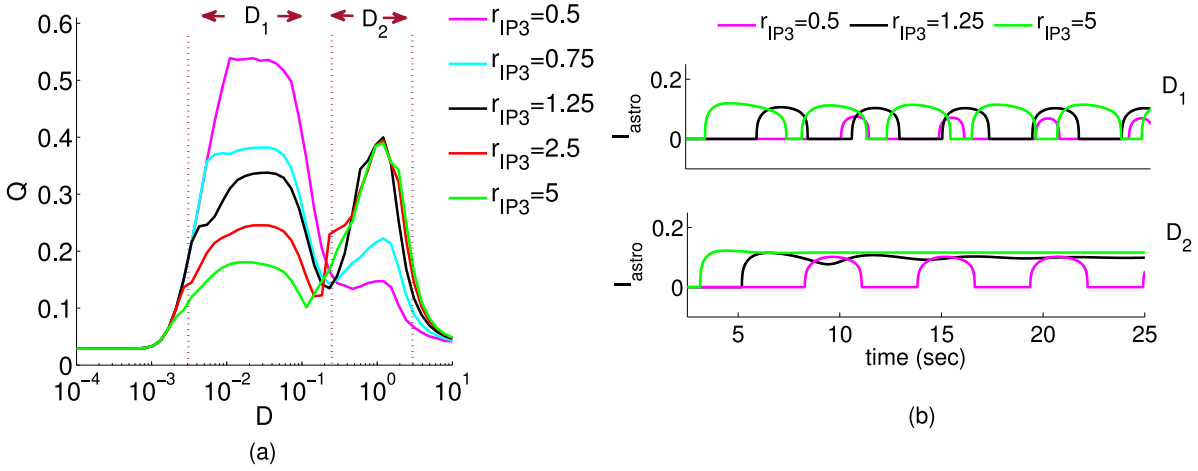

Fig. 5. The weak signal detection performance of the dressed neuron for various $IP3$ production rates. (a) Q versus D for different values of r_{IP3} and a fixed $\lambda = 0.009$. (b) Astrocytic feedback profiles for different r_{IP3} in D_1 and D_2 noise regions marked in panel (a). The feedback profiles are shown for the three considered r_{IP3} values that are the same color coded with the SR curves in the left panel. (For interpretation of the references to color in this figure legend, the reader is referred to the web version of this article.)

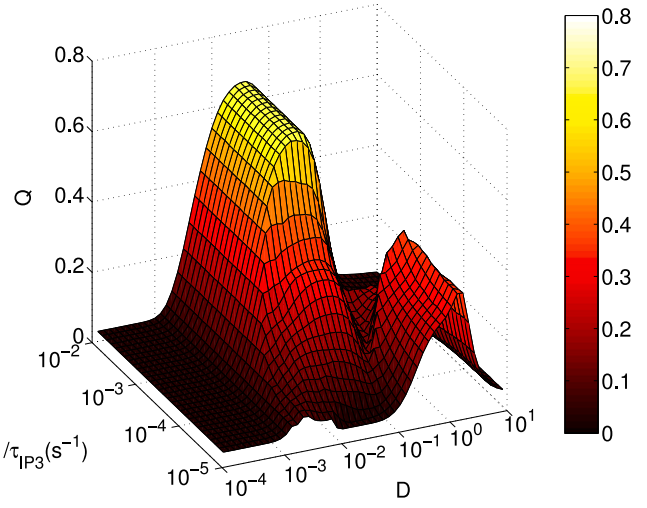

Fig. 6. Fourier coefficient Q in parameter space D and $1/\tau_{IP3}$. As seen in the 3D plot, the neuron elicits single or double resonance behavior on D axis, depending on decay constant τ_{IP3}. The other astrocyte parameters and subthreshold signal parameters are at their default values. (ω_s =1.42, A=0.01, λ=0.009 and r_{IP3}=1.25). (For interpretation of the references to color in this figure legend, the reader is referred to the web version of this article.)

I_{astro}, and then the dressed neuron exhibits classical SR behavior as in the isolated neuron state. On the other hand, $IP3$ diffusion on a fast temporal scale (i.e. when τ_{IP3} is small) can leads to the strong release of Ca^{2+} from intracellular stores even if the neuron fires a small number of spikes. Thus, when the noise level is low, the dressed cell remains silent for a long time due to the high level of astrocyte inhibitory feedback and then the weak signal detection performance of the system becomes low due to the sparse firing activity. As the noise level increases, the phase-locked mode emerges between the dressed neuron's membrane trace and the weak input signal, as the inhibitory effect of the astrocyte is not sufficient to silence neuronal activity at such these noise level. So far we have set the τ_{IP3} value at a constant optimal level and our analyses showed that the astrocytic feedback can induce double resonance behavior when τ_{IP3} is in the optimal range and other parameters are properly adjusted. Fig. 6 also supports these findings and it demonstrates that τ_{IP3} is a relevant parameter to control the impact of the noise on SR phenomenon by providing single or double SR behaviors.

4. Discussion

In summary, we have numerically investigated the effect of an astrocyte on the stochastic resonance behavior of a neuron that is initially subject to a source of uncorrelated noise. To do so, we used a bipartite model that includes a neuron and an astrocyte and explored the output of the neuron in response to a weak periodic input signal.

First, for comparison, we illustrated that the system exhibits the classical SR behavior for the isolated neuron case in which the neuron is not coupled with the astrocyte dynamics. Then, we showed that the inherent dynamics of the astrocyte can lead to emergence of double SR behavior in neuron's dynamics via the astrocytic feedback which modulates synaptic transmission by changing the frequency of neuronal firing. To explain the origin of intriguing crosstalk among these two different cell types, we focused on the properties of the astrocytic feedback, I_{astro}, that can vary in amplitude and width depending on relevant parameters of the astrocyte dynamics and on the different presynaptic neuron firing modes. More precisely, our model shows how the voltage of the presynaptic neuron acts on the astrocyte calcium dynamics via several processes including glutamate release at the synapse and posterior uptake by the astrocyte and IP3 production. Then, after calcium induced gliotransmitter release, it generates I_{astro} through A1R channels in the presynaptic neuron which affects the distance to its firing threshold and then modulating its firing pattern. Moreover, we showed that such astrocyte modulated firing activity of this dressed neuron leads to a second resonance peak by exhibiting phase-locked activity with the weak signal input at high levels of noise intensity.

Finally, in order to observe what would be the impact of neuron–astrocyte coupling strength and astrocyte intrinsic dynamics on such double SR, we analyzed in detail each relevant parameter. Our explorations about the effects of the astrocyte–neuron coupling strength, $IP3$ production and degradation rate on double SR reveal that the double SR behavior may occur over some specific parameter ranges, and it changes smoothly into classical SR behavior outside these ranges.

Our main findings here present a foresight about the potential effect of astrocyte on weak signal detection and transmission in neural systems which include neuron and astrocyte cooperation. Therefore, the present study can be extended to study the effects of astrocyte dynamics on different types of resonance phenomena in complex networks topologies including neurons and astrocyte as basic elements. We hope that our results could be helpful for further understanding the important roles which are served by astrocytes in neural information processing.

Declaration of competing interest

The authors declare that they have no known competing financial interests or personal relationships that could have appeared to influence the work reported in this paper.

Data availability

No data was used for the research described in the article.

Acknowledgments

M.U. acknowledges support of the ERASMUS Program for his research stay in Slovenia. M.P. was supported by the Slovenian Research Agency (Grant Nos. P1-0403 and J1-2457). J.J.T. acknowledges financial support from the Consejería de Transformación Económica, Industria, Conocimiento y Universidades, Spain, Junta de Andalucía, Spain and European Regional Development Funds, Ref. P20_00173. This work is also part of the Project of I+D+i, Spain Ref. PID2020-113681GB-I00, financed by MICIN/AEI/10.13039/501100011033 and FEDER, Spain "A way to make Europe".

References

[1] Janson N. Contemp Phys 2012;53(2):137–68.
[2] Stoof R, Goni-Moreno Á. J R Soc Interface 2022;17(172):20200561.
[3] Berger TW, Song D, Chan RH, Marmarelis VZ. Proc IEEE 2010;98(3):356–74.
[4] Oldham S, Fornito A. Dev Cogn Neurosci 2019;36:100607.
[5] He F, Yang Y. Neuroscience 2021;458:213–28.
[6] Hanggi P. Chemphyschem 2002;3:285–90.
[7] Wiley RH. Adv Study Behav 2006;36:217–47.
[8] Faisal AA, Selen LPJ, Wolpert DM. Nat Rev Neurosci 2008;9(4):292–303.
[9] Luther D, Genty K. Behaviour 2013;150:1045–68.
[10] Fink CG. Amer J Phys 2018;86(11):805–17.
[11] Ward LM, MacLean SM, Kirschner A. PLoS ONE 2010;5:e14371.
[12] Ge L, Liu XD. Acta Pharmaceutica Sinica 2016;37(1):67–74.
[13] Sorokin V, Blekhman I. European J Appl Math 2018;30(5):986–1003.
[14] Agaoglu SN, Calim A, et al. Neurocomputing 2019;325:59–66.
[15] Baysal V, Erkan E, Yilmaz E. Phil Trans R Soc A 2021;379:20200237.
[16] Verones F, Milott E. Eur J Phys 2022;43:025703.
[17] Mejias JF, Torres JJ. PLoS ONE 2011;6(3):e17255.
[18] Yilmaz E, Uzuntarla M, Ozer M, et al. Phys A 2013;392:5735–41.
[19] Castellanos AP. 2018, arXiv:1810.06731.
[20] Nobusako S, Matsuo M, Fukuchi T, et al. PLoS One 2018;13(12):025703, e0209382.
[21] Calim A, Palabas T, Uzuntarla M. Phil Trans R Soc A 2021;379(2198):20200236.
[22] Harikrishnan NB, Nithin N. Neural Netw 2021;143:425–35.
[23] Kosko B, Mitaim S. Phys Rev E 2001;64:051110.
[24] Torres JJ, Marro J, Mejias JF. New J Phys 2011;13:053014.
[25] Pinamonti G, Marro J, Torres JJ. PLoS One 2012;7:e51170.
[26] Torres JJ, Elices I, Marro J. Int J Complex Syst Sci 2013;3:21–5.
[27] Torres JJ, Elices I, Marro J. PLoS One 2015;10(3):0121156.
[28] Li H, Sun X, Xiao J. Chaos 2018;28:043113.
[29] Zao J, Qin Y, Che Y, et al. Cogn Neurodyn 2020;14:399–409.
[30] Li T, Wu K, Yan M, et al. Internat J Modern Phys B 2021;35(10):2150137.
[31] Yamakou ME, Tran TD. Nonlinear Dynam 2022;107:2847–65.
[32] Schmid G, Goychuk I, Hanggi P. Europhys Lett 2001;56(1):22–8.
[33] Adair RK. Proc Natl Acad Sci U S A 2003;100:12099–104.
[34] Perc M. Phys Rev 2007;76(6):066203.
[35] Wang Q, Perc M, Duan Z, Chen G. Chaos 2009;19(2):023112.
[36] Guo DQ, Perc M, Liu TJ, Yao DZ. Europhys Lett 2018;124(5):50001.
[37] Lee CCJ, Anton M, Poon CS. J Comput Neurosci 2009;26:459.
[38] Knoll G, Linder B. J Comput Neurosci 2021;49:407–18.
[39] Hu Z, Wang J, Hao X, et al. Nonlinear Dynam 2022;108:2731–49.
[40] Torres JJ, Elices I, Marro J. PLoS ONE 2015;10(3):e0121156.
[41] Zhao J, Deng B, Qin YJ. Cogn Neurodyn 2017;11:81–90.
[42] Hou JG, Lin Leu-Fen H, Mytilineou C. J Neurochemisty 1996;66:74–82.
[43] Allen NJ, Lyons DA. Science 2018;362(6411):181–5.
[44] Barber CN, Raben DM. Front Cellular Neurosci 2019;13:212.
[45] Poyhonen S, Domanskyi A, Airavaara M. Front Physiol 2019;10:486.
[46] Van Horn MR, Ruthazer ES. Curr Opin Neurobiol 2019;54:113–9.
[47] Ibrahim AM, Pottoo FH, et al. Eur J Neurosci 2020;52(2):2931–43.
[48] Sancho L, Contreras M, Allen NJ. Neurosci Res 2021;167:17–29.
[49] Shan L, Zhang T, Fan K, et al. Front Cell Dev Biol 2021;9:1786.
[50] De Pitta M, Goldberg M, et al. J Biol Phys 2009;35:383–411.
[51] Erkan Y, Sarac Z, Yilmaz E. Nonlinear Dynam 2019;95:3411–21.
[52] Calim A, Longtin A, Uzuntarla M. Philos Trans R Soc A 2021;379(2198):20200267.
[53] Palabas T, Longtin A, Ghosh D, Uzuntarla M. Chaos 2022;32(5):051101.
[54] Parpura V, Zorec R. Brain Res Rev 2010;63(1–2):83–92.
[55] Harada K, Kamiya T, Tsuboi T. Front Neurosci 2016;9:499.
[56] Satarker S, Bojja SL, Gurram PC, Mudgal J, Arora D, Nampoothiri M. Cells 2022;11(7).
[57] Liu Y, Li CG. J Theoret Biol 2013;335:265–75.
[58] Erkan Y, Saraç Z, Yilmaz E. Nonlinear Dynam 2019;95:3411–21.
[59] Qiao Z, Liu J, et al. J Franklin Inst B 2021;35(3):2194–211.
[60] FitzHugh R. Biophys J 1961;1:445.
[61] Postnov DE, Ryazanova LS, Sosnovtseva OV. BioSystems 2022;89(1–3):887–97.
[62] Postnov DE, Koreshkov RN, et al. J Biol Phys 2009;35:425–45.
[63] Abbott LF, Kepler TB. Statistical mechanics of neural networks lecture notes in physics. Vol. 368, 1990, p. 5–18.
[64] Brown P, Dale N. J Physiol 2000;525:655.
[65] Rotermund N, Winandy S, et al. J Physiol 2018;596(4):717–33.
[66] Nadkarni S, Jung P. Phys Rev Lett 2003;91:268101.
[67] Wang SS, Alousi AA, Thompson SH. J Gen Physiol 1995;105:149–71.
[68] De Young GW, Keizer J. Proc Natl Acad Sci U S A 1992;89(20):9895.
[69] Ullah G, Jung P. Cornell-Bell, Cell Calcium 2006;39:197.
[70] Amiri M, Montaseri G, Bahrami F. Biol Cybernet 2011;105:153–66.
[71] Li Y, Rinzel J. J Theoret Biol 1994;166:461–73.
[72] Manninen T, Havela R, Linne M-L. Front Comput Neurosci 2017;12(14).
[73] Volman V, Ben-Jacob E, Levine H. Neural Comput 2007;19:303–26.
[74] Ozer M, Perc M, Uzuntarla M. Phys Lett A 2009;373(10):964–8.
[75] Yao Y, Ma J. Cogn Neurodyn 2018;12(3):343–9.
[76] Longtin A. Chaos 1995;5(1):209–15.
[77] Yang L, Liu W, et al. Phys Rev E 2012;86(1):016209.
[78] Nadkarni S, Jung P. Phys Biol 2004;1(1):35.